**ORIGINAL ARTICLE**

# Neutrophil extracellular traps drive epithelial–mesenchymal transition of human colon cancer

Antonia M Stehr[1], Guangxia Wang[1], Richard Demmler[1], Marc P Stemmler[2], Julia Krug[1], Philipp Tripal[3], Benjamin Schmid[3], Carol I Geppert[4], Arndt Hartmann[4], Luis E Muñoz[5,6], Janina Schoen[5,6], Simon Völkl[7], Susanne Merkel[8], Christoph Becker[9], Georg Schett[5,6], Robert Grützmann[8], Elisabeth Naschberger[1], Martin Herrmann[5,6†] and Michael Stürzl[1,10†*]

[1] Division of Molecular and Experimental Surgery, Translational Research Center, Department of Surgery, Friedrich-Alexander University (FAU) Erlangen-Nürnberg and Universitätsklinikum Erlangen, Erlangen, Germany
[2] Department of Experimental Medicine 1, Nikolaus-Fiebiger Center for Molecular Medicine, Friedrich-Alexander University (FAU) Erlangen-Nürnberg, Erlangen, Germany
[3] Optical Imaging Centre, Friedrich-Alexander University (FAU) Erlangen-Nürnberg, Erlangen, Germany
[4] Institute of Pathology, Friedrich-Alexander University (FAU) Erlangen-Nürnberg and Universitätsklinikum Erlangen, Erlangen, Germany
[5] Department of Internal Medicine 3, Friedrich-Alexander University (FAU) Erlangen-Nürnberg and Universitätsklinikum Erlangen, Erlangen, Germany
[6] Deutsches Zentrum für Immuntherapie (DZI), Friedrich-Alexander University (FAU) Erlangen-Nürnberg and Universitätsklinikum Erlangen, Erlangen, Germany
[7] Department of Internal Medicine 5, Friedrich-Alexander University (FAU) Erlangen-Nürnberg and Universitätsklinikum Erlangen, Erlangen, Germany
[8] Department of Surgery, Friedrich-Alexander University (FAU) Erlangen-Nürnberg and Universitätsklinikum Erlangen, Erlangen, Germany
[9] Department of Internal Medicine 1, Friedrich-Alexander University (FAU) Erlangen-Nürnberg and Universitätsklinikum Erlangen, Erlangen, Germany
[10] Comprehensive Cancer Center Erlangen-EMN, Universitätsklinikum Erlangen, Erlangen, Germany

*Correspondence to: M Stürzl, Friedrich-Alexander University (FAU) of Erlangen-Nürnberg, Universitätsklinikum Erlangen, Department of Surgery, Translational Research Center, Division of Molecular and Experimental Surgery, Schwabachanlage 12, 91054 Erlangen, Germany. E-mail: michael.stuerzl@uk-erlangen.de

†These authors jointly supervised this work.

## Abstract

Neutrophil extracellular traps (NETs) are extracellular structures, composed of nuclear DNA and various proteins released from neutrophils. Evidence is growing that NETs exert manifold functions in infection, immunity and cancer. Recently, NETs have been detected in colorectal cancer (CRC) tissues, but their association with disease progression and putative functional impact on tumourigenesis remained elusive. Using high-resolution stimulated emission depletion (STED) microscopy, we showed that citrullinated histone H3 (H3cit) is sufficient to specifically detect citrullinated NETs in colon cancer tissues. Among other evidence, this was supported by the close association of H3cit with de-condensed extracellular DNA, the hallmark of NETs. Extracellular DNA was reliably differentiated from nuclear condensed DNA by staining with an anti-DNA antibody, providing a novel and valuable tool to detect NETs in formalin-fixed paraffin-embedded tissues. Using these markers, the clinical association of NETs was investigated in a cohort of 85 patients with colon cancer. NETs were frequently detected (37/85, 44%) in colon cancer tissue sections and preferentially localised either only in the tumour centre or both in the tumour centre and the invasive front. Of note, citrullinated NETs were significantly associated with high histopathological tumour grades and lymph node metastasis. *In vitro*, purified NETs induced filopodia formation and cell motility in CRC cell lines. This was associated with increased expression of mesenchymal marker mRNAs (vimentin [*VIM*], fibronectin [*FN1*]) and epithelial–mesenchymal transition promoting transcription factors (*ZEB1,* Slug [*SNAI2*]), as well as decreased expression of the epithelial markers E-cadherin (*CDH1*) and epithelial cell adhesion molecule (*EPCAM*). These findings indicated that NETs activate an epithelial–mesenchymal transition-like process in CRC cells and may contribute to the metastatic progression of CRC.
© 2021 The Authors. *The Journal of Pathology* published by John Wiley & Sons Ltd on behalf of The Pathological Society of Great Britain and Ireland.

Keywords: colorectal neoplasms; extracellular traps; neutrophils; stimulated emission depletion (STED) microscopy; migration; epithelial–mesenchymal transition (EMT)

## Introduction

Colorectal cancer (CRC) is the third most common cancer type worldwide, in both men and women, and holds the fifth highest mortality rate among all malignancies [1]. Immune cell infiltration is highly associated with the outcome of the disease [2]. Furthermore, the identification of consensus molecular subtypes (CMS) showed that certain immune cell signatures are associated with mortality of patients with CRC [3]. Specifically, the unfavourable, 'mesenchymal' (CMS4) subtype of CRC was characterised by increased expression of immuno-suppressive factors and chemoattractants, as well as the infiltration of innate immune cells [4]. In a novel metastatic CRC mouse model, tumours resembling the CMS4 subtype showed an increased neutrophil accumulation as compared with prognostically favourable CMS1–3 tumours [4].

Neutrophils are the most abundant type of innate immune cells in humans, acting as a first-line defence against pathogens [5]. Neutrophils exert their functions by phagocytosis, degranulation and the formation of neutrophil extracellular traps (NETs) [6]. NETs are extracellular structures, composed of nuclear DNA and various proteins released from neutrophils, most prominently represented by histones and granular enzymes, such as neutrophil elastase (NE) and myeloperoxidase (MPO) [6]. Neutrophils undergo several morphological changes during the formation of NETs. Initially, the nuclei of activated neutrophils lose their characteristic lobules, then chromatin begins to de-condense, while the nuclear membrane remains intact [7]. Part of this process is the citrullination of histones, catalysed by peptidylarginine-deiminase 4 (PAD4). Citrullination changes the charge and initiates the de-condensation of nuclear chromatin [8]. Eventually, both the nuclear and the granular membranes lose their integrity, allowing NET components to mix, which results in the disruption of the plasma membrane and the release of the NETs into the extracellular space [7].

NETs have first been described as a mechanism to trap and kill bacteria [6]. In recent years, however, evidence has accumulated of NETs negatively influencing various, also non-infectious, diseases. Among these are thrombotic events [9–12], pre-eclampsia [13], sepsis [14] and, most recently, the coagulopathy, organ damage and immunothrombosis that characterise severe cases of COVID-19 [15]. The first evidence for NETs playing a role in cancer was provided by a study on a small cohort of patients ($n = 8$) with paediatric Ewing sarcoma in 2013, suggesting that NETs might be associated with metastasis and early relapse [16]. Since then, various studies have connected NETs with cancer metastasis and progression. However, only a few focused on intra-tumour NETs [17–20].

The assessment of intratumour NET formation remains difficult, as there is no high-fidelity protocol for examining the presence of NETs in tissue samples. Most studies use a combination of different markers to show the presence of NETs. For example, in intact neutrophils, nuclear histones and cytoplasmic granular enzymes reside in separated compartments. NET formation leads to co-localisation of these proteins and the extracellular DNA in the NETs. This suggested that specific detection of NETs can be achieved by analysis of the co-localisation of extracellular DNA and histone H2B with granular proteins, such as NE and MPO [21]. In addition, several studies described a critical role of PAD4-dependent citrullination in NET formation, showing that inhibition of PAD4 reduced chromatin de-condensation and NET formation *in vitro* [22] and *in vivo* [23]. On this basis, citrullinated histone H3 (H3cit) is frequently used as a marker for NETs, both in single and combined staining protocols. Recently, multiplex immunofluorescence analyses have been reported, to detect NETs in CRC in small groups of 10 or 20 patients [24,25]. However, the association of NETs with specific clinical features in CRC remained elusive. Here, we used high-resolution stimulated emission depletion (STED) microscopy to identify the most appropriate and easily usable marker for the detection of NETs in human formalin-fixed paraffin-embedded (FFPE) tissues sections from colon cancer tissues and applied this approach to investigate the clinical association of NETs in a cohort of 85 patients with colon cancer. Finally, we determined whether NETs may directly act on the tumour cells inducing a phenotype, which could explain the appearance of clinical features associated with NETs in CRC.

## Materials and methods

### Ethics approval

The study was performed in accordance with the Declaration of Helsinki after approval of all procedures by the local ethics committee of the Friedrich-Alexander University (FAU) Erlangen-Nuremberg, Germany (no. 159_15 B, 26.10.2020 [tumour specimen]; no. 243_15 B, 16.03.2017 [neutrophil isolation]). Patients and healthy volunteers gave written informed consent before participation in this study.

### Patients

Human CRC tissues were retrieved as FFPE blocks after completion of routine diagnostics as a retrospective study cohort from the Institute of Pathology, Friedrich-Alexander University (FAU) Erlangen-Nürnberg. The inclusion criteria were patients with first manifestation of histologically verified colon cancer (stage UICC I–IV) [26]. Exclusion criteria were patients with hereditary tumours (hereditary non-polyposis colorectal cancer (HNPCC), familial adenomatous polyposis (FAP)) or tumours resulting from inflammatory bowel disease (ulcerative colitis, Crohn's disease). The detailed patient characteristics are given in Table 1.

Neutrophils were isolated from the blood of healthy volunteers.

Table 1. Patients included for evaluation of NET formation in colon cancer (n = 85).

|  | n | % |
|---|---|---|
| Sex ratio (male/female) | 49/36 = 1.36 |  |
| Age (years) |  |  |
| Mean | 68.15 |  |
| <50 | 4 | 4.7 |
| 50–59 | 15 | 17.4 |
| 60–69 | 20 | 22.1 |
| 70–79 | 38 | 46.5 |
| ≥80 | 8 | 9.3 |
| Stage (UICC) |  |  |
| I | 20 | 23.5 |
| II | 22 | 25.9 |
| III | 22 | 25.9 |
| IV | 21 | 24.7 |
| Primary tumour (UICC) |  |  |
| pT1 | 4 | 4.7 |
| pT2 | 19 | 22.4 |
| pT3 | 48 | 56.5 |
| PT4 | 14 | 16.5 |
| Histopathological grading |  |  |
| Low grade (1/2) | 56 | 65.9 |
| High grade (3/4) | 29 | 34.1 |
| Regional lymph nodes (UICC) |  |  |
| pN– | 45 | 52.9 |
| pN+ | 40 | 47.1 |
| Lymphatic vessel invasion |  |  |
| No | 44 | 51.8 |
| Yes | 41 | 48.2 |
| Distant metastasis |  |  |
| M– | 64 | 75.3 |
| M+ | 21 | 24.7 |
| Histological classification (WHO) |  |  |
| Adenocarcinoma | 75 | 88.2 |
| Mucinous adenocarcinoma | 10 | 11.8 |
| Tumour site |  |  |
| Coecum | 19 | 22.4 |
| Colon ascendens | 19 | 22.4 |
| Flexura hepatica | 6 | 7.1 |
| Colon transversum | 8 | 9.4 |
| Flexura lienalis | 1 | 1.2 |
| Colon descendens | 6 | 7.1 |
| Sigma | 26 | 30.6 |
| H3cit positivity |  |  |
| Negative | 48 | 56.5 |
| Positive | 37 | 43.5 |

## Tissue staining and H3cit scoring

Immunostaining was carried out as described recently [27,28]. FFPE tissue sections (4 μm) were de-paraffinised and rehydrated before performing target retrieval at pH 9.0 (DakoCytomation/Agilent, Santa Clara, CA, USA) and 70 °C for 120 min for NE and H2B staining or pH 6.0 (DakoCytomation/Agilent) and 90 °C for 20 min for DNA and H3cit staining [21]. After permeabilisation with 0.5% Triton in 1 × TBS for 6 min and blocking with 10% normal serum (Dianova, Hamburg, Germany) + 2% BSA (Sigma-Aldrich, Saint Louis, MO, USA) + 0.1% Triton X-100 (Sigma-Aldrich) + 0.05% Tween 20 (Sigma-Aldrich) in 1 × TBS for 1 h at room temperature, primary antibodies (anti-ELANE antibody, #HPA066836, Atlas Antibodies, Bromma, Sweden, polyclonal IgG, 1:100; anti-

histone H2B antibody, #ab134211, Abcam, Cambridge, UK, polyclonal IgY, 1:1,000; anti-DNA antibody, #CBL186, Merck, Billerica, MA, USA, monoclonal IgM, 1:100; anti-H3cit antibody, #ab5103, Abcam, polyclonal IgG, 1:150) were applied overnight at 4 °C. Secondary antibodies for confocal and epifluorescence microscopy (Cy™2-conjugated donkey anti-rabbit, #711–225-152, Jackson ImmunoResearch, Ely, UK, 1:400; Cy™3-conjugated donkey anti-chicken, #703–165-155, Jackson ImmunoResearch, 1:400; Alexa Fluor 647 goat anti-mouse, #A2179865, ThermoFisher, Waltham, MA, USA, 1:100; Alexa Fluor 546 goat anti-rabbit, #A11035, ThermoFisher, 1:500) or STED microscopy (Abberior Star orange goat anti-chicken, Abberior, Göttingen, Germany, 1:200; Abberior Star 635P goat anti-rabbit, Abberior, 1:200; Abberior Star 580 goat anti-rabbit, Abberior, 1:200; Alexa Fluor 647 goat anti-mouse, #A2179865, ThermoFisher, 1:100) were incubated for 1 h at room temperature. Counterstaining with DAPI (ThermoFisher) and Draq5 (Cell Signaling Technology, Danvers, MA, USA) was carried out before mounting. Isotype control staining for each antibody was carried out on consecutive sections. Staining was analysed using a laser scanning microscope (DMI4000 B, Leica, Wetzlar, Germany). For STED microscopy, a STED facility line microscope (Abberior STED 2-Channel Super Resolution Microscope) was used. H&E staining was carried out on a further consecutive section and assessed using a bright field microscope (DM600 B, Leica).

Scoring for H3cit positivity was carried out blind (without knowledge of the clinical parameters) by two persons independently. In cases of disagreement, discussion to consent was made. The tissue sections of all patients were assessed using a fluorescence (DM6000B, Leica) microscope and classified into H3cit-positive and -negative tumours. Positive areas that were separated from the tumour section or only found at the outermost edge of the tissue were not included. Isotype control-stained sections were used to validate the signal specificity.

## Neutrophil isolation and induction of NET formation

EDTA-blood from healthy human donors was drawn and neutrophils were isolated using a Ficoll-Diatrizoate density gradient (Lymphoflot, Biorad, Hercules, CA, USA, #824012) and incubated with 500 nM phorbol 12-myristate 13-acetate (PMA, Sigma-Aldrich, #P1585) for 4 h at 37 °C to allow NET formation. NETs were collected, pelleted and resuspended in 1 × PBS according to a protocol published by Najmeh et al [29]. The concentration of this NET stock was quantified using a NanoDrop spectrophotometer (ThermoFisher).

### Calculation of PMA dilution in NETs stock

Initially, the neutrophils were stimulated with 500 nM PMA to induce NETs; after 4 h the PMA-containing medium was discarded and NETs were washed off the

cell culture dish using 5–6 ml 1 × PBS. Approximately, 200 μl PMA-containing medium remained on the dish, resulting in a 25–30-fold dilution of PMA. NETs were pelleted, the supernatant was discarded and the NETs were pooled together in 250–700 μl 1 × PBS, depending on the pellet sizes. Less than 100 μl remained on the pellets, resulting in a further 3.5–9-fold dilution of PMA. For treatment of the cells, the NET stock was diluted to 500 ng/ml in cell culture medium. Depending on the initial NET concentration, the range of dilution at this step was 1:314–1:1,095. In total, this resulted in a 30,000–176,000-fold dilution of the initially added PMA when NETs were applied onto the cells. Accordingly, the maximum concentration of residual PMA was 0.016 nM. For the quantification experiments (Figures 4C, 5A,B and supplementary material, Figure S1), a NET stock requiring an 82,000-fold dilution with a calculated residual PMA concentration of 0.006 nM was used. PMA even in 17-fold higher concentrations did not activate cell migration (see supplementary material, Figure S1).

## Cell culture

DLD1 and SW480 CRC cell lines were purchased from ATCC (Manassas, VA, USA) and authenticated by analysing the DNA profile of 17 highly polymorphic sites of short tandem repeats using multiplex PCR (Leibniz Institute, Deutsche Sammlung von Mikroorganismen und Zellkulturen (DMSZ), Braunschweig, Germany) as described previously [30]. Both cell lines were cultured in RPMI medium (ThermoFisher) + 10% FCS (Merck) + 1% glutamine (ThermoFisher) at 5% $CO_2$ in the absence of antibiotics. Mycoplasma tests (MycoAlert, Lonza, Basel, Switzerland) were carried out on a regular basis and were negative.

For all experiments, cells were seeded in full medium (10% FCS), after firm adhesion cultured in the absence of FCS for 10 h and subsequently stimulated for the indicated time periods.

## Time–lapse microscopy

Time-lapse microscopy was conducted in 24-well plates (ThermoFisher) using phase-contrast microscopy (DMI4000 B, Leica) and an automatically controlled stage and incubation system (5% $CO_2$, 37 °C). Cells were seeded (DLD1: 15,000 cells/well; SW480: 20,000 cells/well) and stimulated with 500 ng/ml NET stock, corresponding volumes of PBS or different concentrations of PMA as controls. Pictures were taken every 10 min for a total duration of 24 h. Videos were processed using ImageJ software.

## Wound healing assays

Cell migration was analysed using wound healing assays, following established methodology [31]. DLD1 and SW480 cells were seeded in triplicate into six-well plates (ThermoFisher, SW480: $1.2 \times 10^6$ cells/well, DLD1: $1 \times 10^6$ cells/well) and stimulated with (1) 500 ng/ml purified NETs, (2) an identical

concentration of DNase-digested or DNase-digested and heat-denatured NETs, (3) a corresponding volume of 1 × PBS as a control or (4) different concentrations of PMA (Sigma-Aldrich). For DNase digestion, the NET stock was incubated with 2 U/μl DNase I (Roche, Rotkreuz, Switzerland) at 37 °C for 30 min and for denaturation of proteins NETs were incubated at 95 °C for 20 min. The scratch was formed using a 1 ml pipet tip and images of identical areas were taken at time points 0, 2, 4, 6, 8, 10, 12, 18 and 24 h for DLD1 cells and at time points 0, 2, 4, 6, 8, 10 and 12 h for SW480 cells using phase-contrast microscopy (Axiovert 25, Zeiss, Oberkochen, Germany). Quantification of open areas was carried out using ImageJ software. To confirm DNase I digestion of NETs, aliquots of the reaction were analysed using 0.8% agarose gel electrophoresis and subsequent ethidium bromide/ultraviolet light visualisation (see supplementary material, Figure S2A).

## Immunofluorescence, western blotting and RT–PCR analyses

Immunofluorescence, western blotting and RT-PCR analyses were conducted following standard procedures and are detailed in Supplementary materials and methods.

## Statistical analyses

### Patient cohort

Statistical differences in clinical parameters were determined using Fisher's exact test.

### Gene expression analysis

Differential gene expression was analysed using two-sided, unpaired *t*-tests corrected using the Holm–Sidak method for multiple comparisons.

### Wound healing assays

Statistical differences in migration between cells in different conditions were analysed by two-sided, paired *t*-test.

# Results

## H3cit and extracellular DNA identify citrullinated NETs in colon cancer

In order to determine how NETs can reliably and most easily be detected in human colon cancer tissues, we stained for NE and H2B on the first and H3cit on the following tissue section, employing immunofluorescence microscopy. Tissue areas showing NE/H2B co-localisation (Figure 1A, arrows) were not in all cases also positive for H3cit (Figure 1A; compare white and red frames, arrowheads). This finding suggested that either H3cit may detect a subpopulation of NETs or NE/H2B co-localisation may also occur in intact neutrophils in the absence of NETs. In order to investigate this,
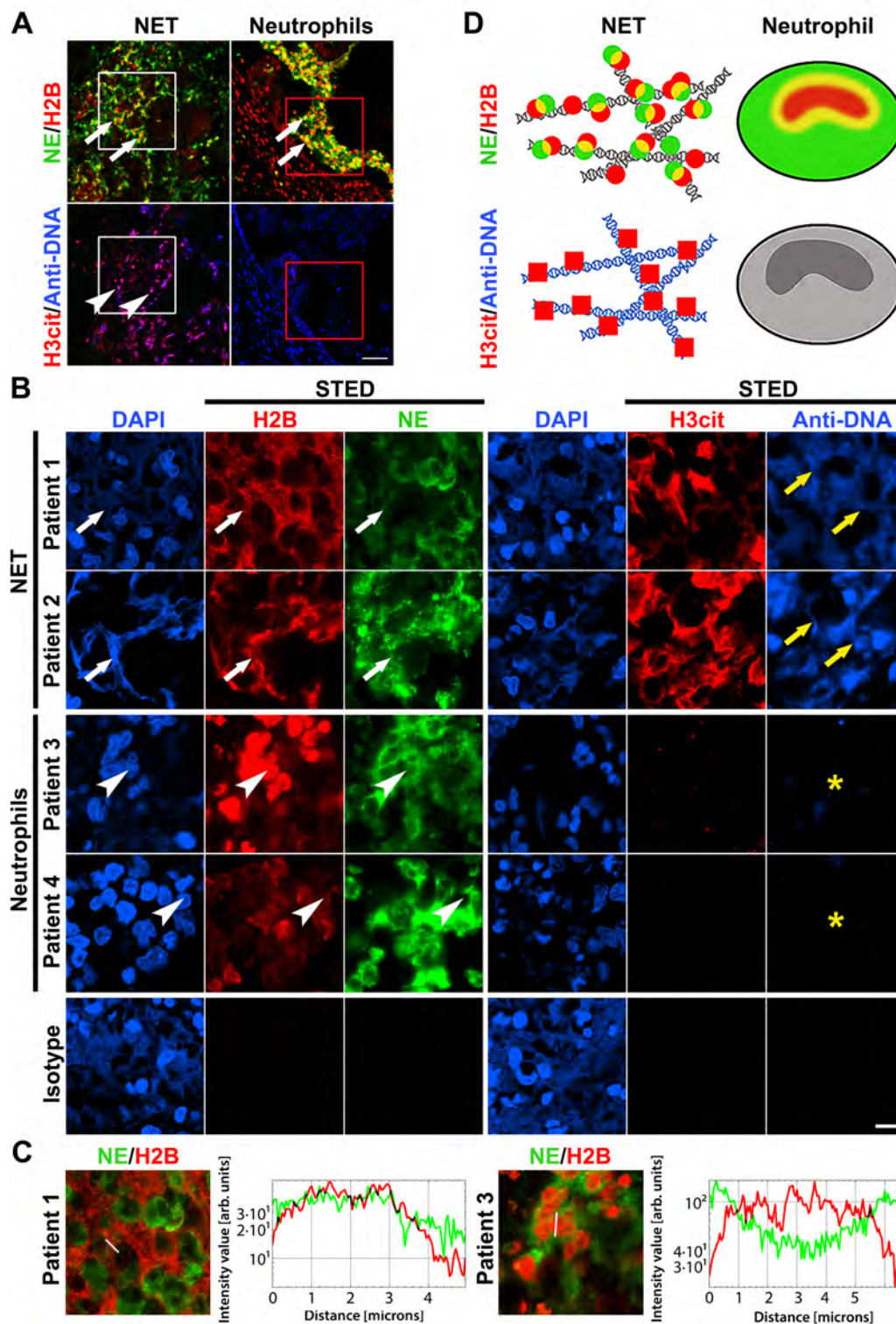
**Figure 1.** Staining of H3cit detected NETs in colon cancer tissue and allowed their differentiation from intact neutrophils. (A) Immunofluorescence staining of H2B, NE, H3cit and DNA (using an anti-DNA IgM antibody) in colon cancer tissues of different patients. NE/H2B double staining and H3cit/DNA double staining were performed on consecutive sections. Confocal microscopy showed that areas of H2B and NE co-localisation (arrows) were not in all cases simultaneously positive for H3cit (arrowheads, compare lower red and white frames). In areas with H3cit/NE/H2B co-staining, DNA signals were stronger (white frames, probably representing NETs) as compared with NE/H2B-positive areas lacking H3cit (red frames, probably representing intact neutrophils). (B) High-resolution imaging via STED. H3cit-positive tissues (patients 1 and 2) showed co-localisation of fibrously and granularly spread NE, H2B and DNA (indicated by DAPI staining; white arrows). In contrast, in H3cit-negative tissues (patients 3 and 4), nuclear DAPI and H2B staining co-localised and NE staining showed cytoplasmic localisation (arrowheads). Staining with an anti-DNA antibody (Anti-DNA) showed intense signals in patients positive for H3cit (yellow arrows) and no or only weak signals in H3cit-negative tissues (asterisks). Isotype controls did not yield any signal. Scale bars: (A) 50 μm; (B) 5 μm. (C) Line profiling of NE and H2B signal intensities of STED images. H3cit-positive tissue of patient 1 showed co-localisation of NE and H2B, as characteristic for NETs. H3cit-negative tissue of patient 3 exhibited the intensity maxima of NE and H2B at different sites, co-localisation was only observed at the nucleocytoplasmic transition zone. (D) Schematic depiction of the signal patterns resulting from NE/H2B and H3cit/DNA double staining in neutrophils and NETs. De-condensed DNA in NETs was strongly stained with the anti-DNA antibody selectively in areas where H3cit was also detected. These areas were also positive for NE and H2B. The coincidence of these four markers specifically identified citrullinated NETs. In contrast, co-staining with NE and H2B also occurred in the nucleocytoplasmic transition zone in intact neutrophils (see also Table 2).
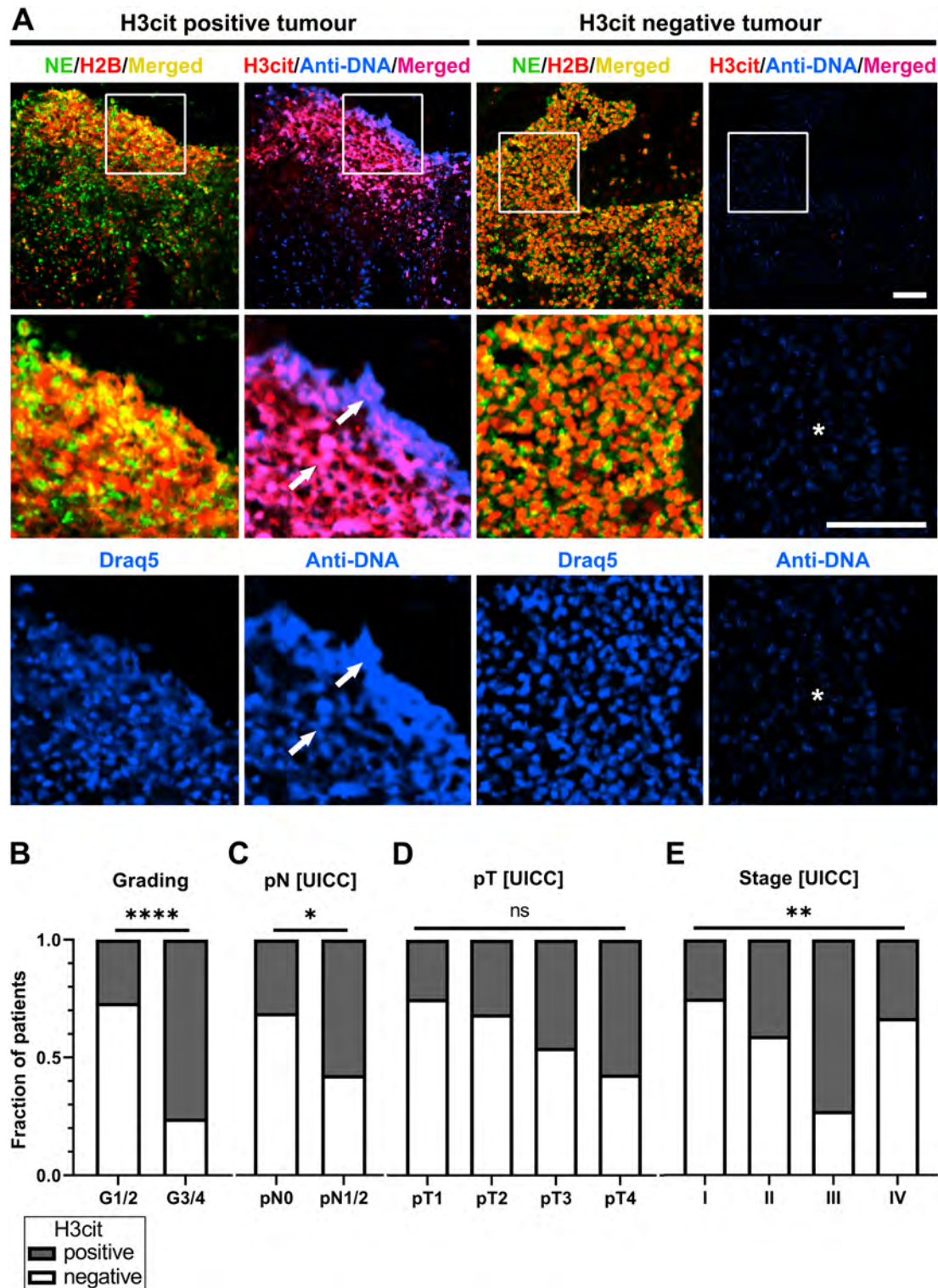
**Figure 2.** High tumour grades and local metastases in colon cancer were associated with citrullinated NETs. (A) NE and H2B, H3cit and DNA (Draq5 and anti-DNA antibody [Anti-DNA]) were stained on consecutive paraffin sections. H3cit-positive areas showed overlapping NE/H2B signals in the corresponding positions of consecutive sections (left panel). Of note, in these areas, strong signals were obtained by staining with the anti-DNA antibody (arrows). In H3cit-negative tissues, overlapping signals for NE and H2B were also obtained, but these areas only displayed no or very weak signals with the anti-DNA IgM antibody (right panel, asterisks). To emphasise the difference in signal intensity between DNA dye (Draq5) and anti-DNA antibody, the anti-DNA channel is shown again without overlapping H3cit signal (lowest panel). For each antibody and patient, a staining with a respective isotype antibody was performed on a consecutive section. This was negative in each case (not shown). Scale bars: 50 μm. (B–E) Quantitative analysis of H3cit staining in colon cancer tissues ($n = 85$) detected citrullinated NETs in 44% (37/85) of the cases. The latter were associated with (B) high histopathological grades and (C) lymph node metastases. (D) A trend of NET formation preferentially present in locally invasive high pT tumours has been observed. The results of (C) and (D) were also reflected in (E) the tumour stage, as most H3cit-positive tumours were either stage II (high pT) or stage III (lymph node metastasis). Statistical significance was determined by Fisher's exact test. ****$p < 0.0001$; **$p < 0.01$; *$p < 0.05$.
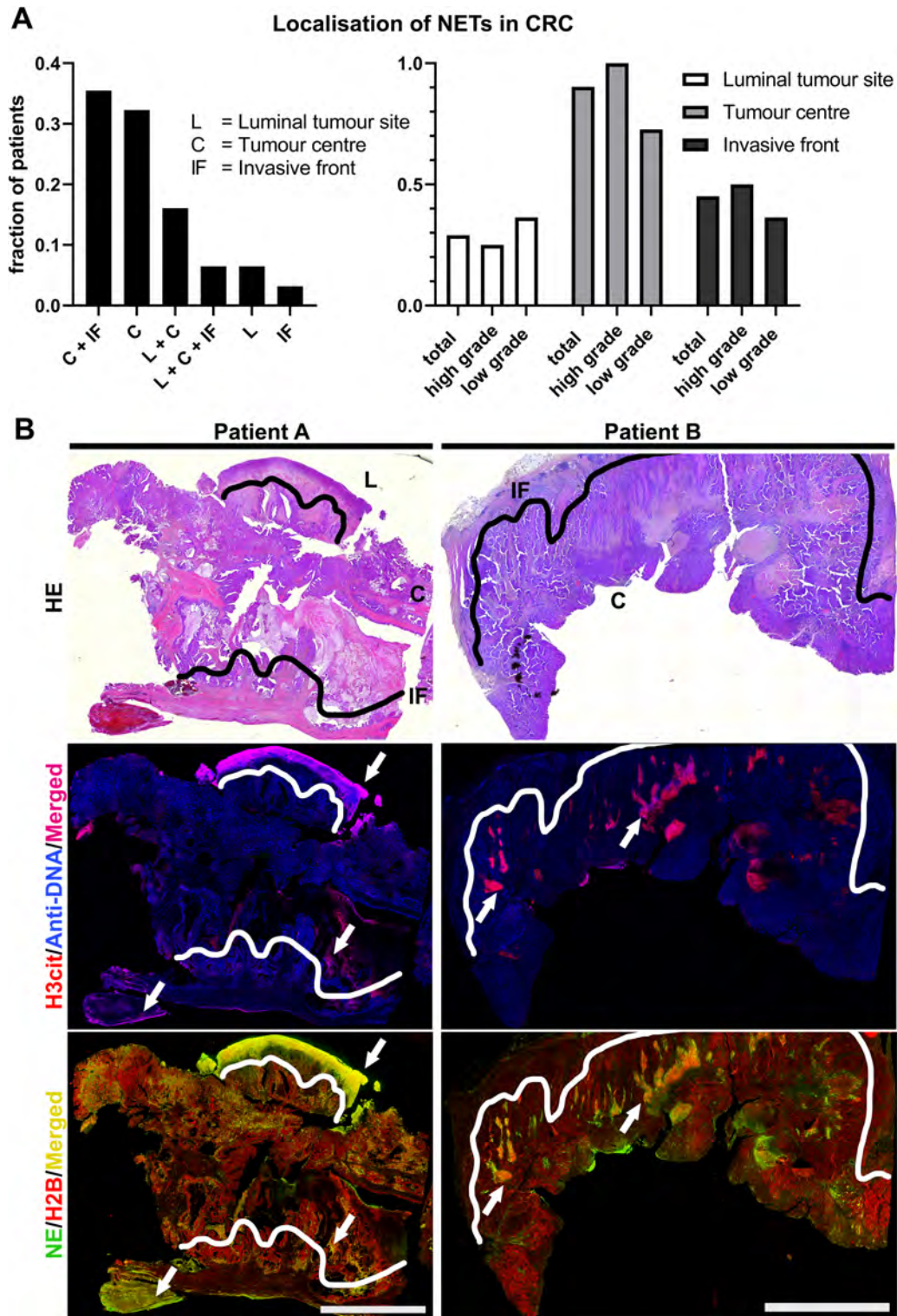
**Figure 3.** NETs were preferentially present in the tumour centre and the invasive front in colon cancer. (A) NETs in colon cancer were preferentially located in the tumour centre and the invasive front (left panel). NET localisation was comparable between high- and low-grade tumours (right panel). The numbers in the right panel show the proportion of NET-positive specimens in the respective groups (total, high grade, low grade). (B) Tile scans of consecutive tissue sections (H&E, NE/H2B, H3cit/DNA). Patient A (left) exhibited NET formation (arrows) in the tumour centre (C), the invasive front (IF) and the luminal side (L) of the tumour. Patient B (right) displayed citrullinated NETs only in the tumour centre (C). Scale bars: 5 mm. Evaluations in (A) and (B) included 31 of the total 37 H3cit-positive patients. For the six missing specimens, the exact localisation of the different tumour sites within the available section could not be determined unequivocally.

NE/H2B-positive specimens with (Figure 1B, patients 1 and 2) and without H3cit presentation (Figure 1B, patients 3 and 4) were subjected to high-resolution

STED microscopy. H2B staining in H3cit-positive tissues was fibrously spread with granular substructures and often co-localised with NE and DNA. The latter
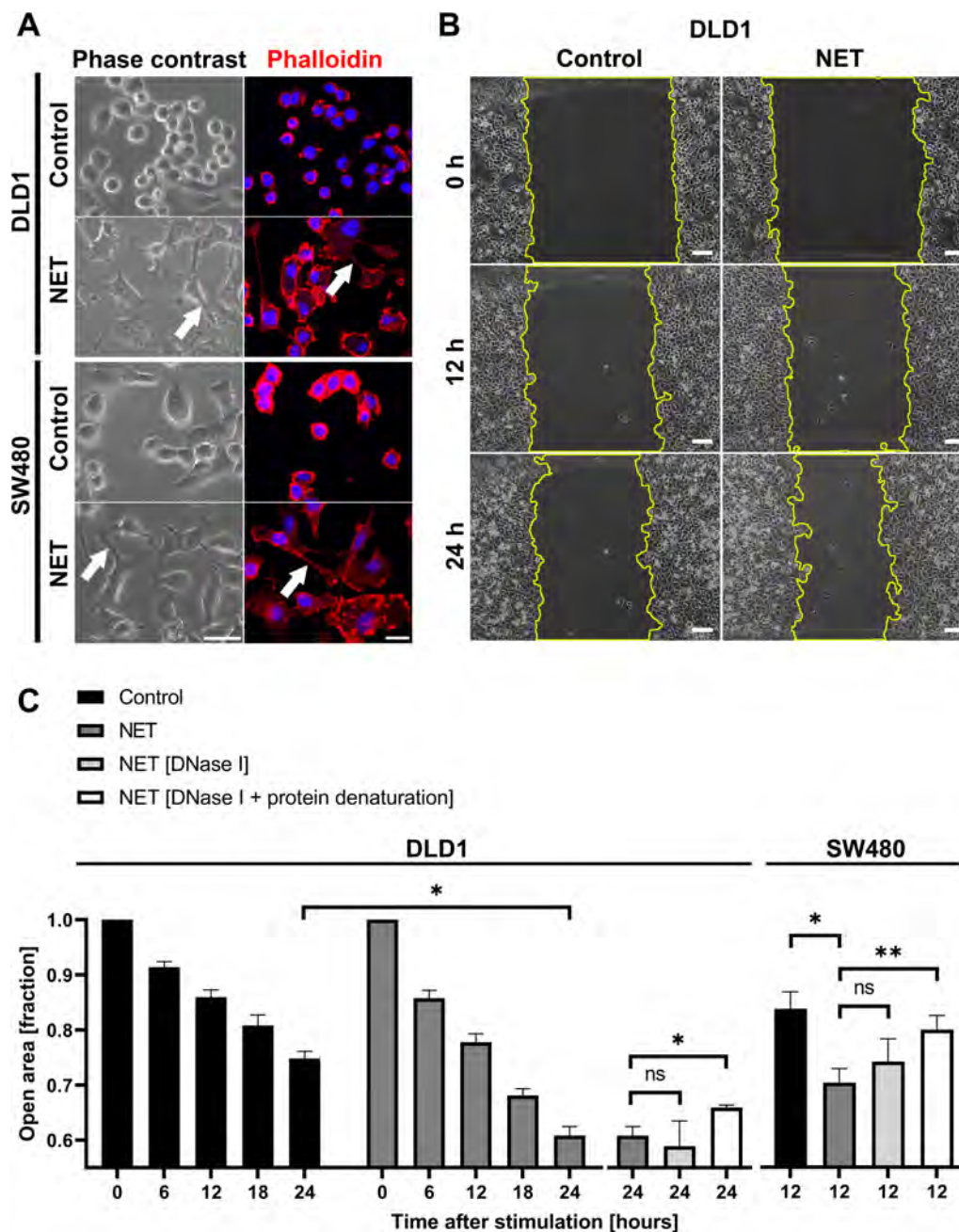
**Figure 4.** NETs increased *in vitro* motility of colon cancer cell lines. (A) Phase contrast images (left panel) and phalloidin staining (right panel) of human CRC cell lines (DLD1, SW480) either unstimulated (Control) or incubated with NETs (500 ng/ml) for 24 h. DNA was stained with nuclear dye (Draq5). The white arrows indicate the formation of pseudopodia. Scale bars correspond to 20 μm. (B and C) Wound healing assay with DLD1 and SW480 cells either untreated (Control) or in the presence of NETs (500 ng/ml). Images were taken at various time points to monitor wound closure. Open areas were determined using the ImageJ software and the quotients of the open areas at certain time points to the open area at time point 0 are shown in the graph (C). Both DLD1 and SW480 exhibited significantly increased migratory activity in the presence of NETs. In both DLD1 and SW480 cells, this effect was partially abrogated by digestion of NETs with 2 U/μl DNase I and subsequent heat denaturation of NET proteins (white bars, C). Digestion of NETs with 2 U/μl DNase I alone did not abrogate the effects of NETs on cell migration (light grey bars, C). Statistical significance was determined using two-sided, paired *t*-test. *$p < 0.05$; **$p < 0.01$. Scale bars correspond to 50 μm.

did not exhibit the typical nuclear morphology as detected with DAPI (Figure 1B, white arrows). In contrast, in specimens lacking H3cit, the H2B staining often co-localised with nuclear DAPI staining, whereas NE displayed a cytoplasmic localisation (Figure 1B, arrowheads). This constellation indicates that H3cit co-localised with extracellular DNA, decorated with NE and H2B, as characteristically observed for NETs. In

contrast, the co-localisation of NE/H2B signals in H3cit-negative areas is prone to be derived from overlapping signals obtained in intact neutrophils at the nucleo-cytoplasmic transition zone. This was further confirmed by staining with an anti-DNA antibody that led to strong signals in H3cit-positive (Figure 1B, patients 1 and 2, yellow arrows) but not H3cit-negative areas (Figure 1B, asterisks). This finding was in agreement
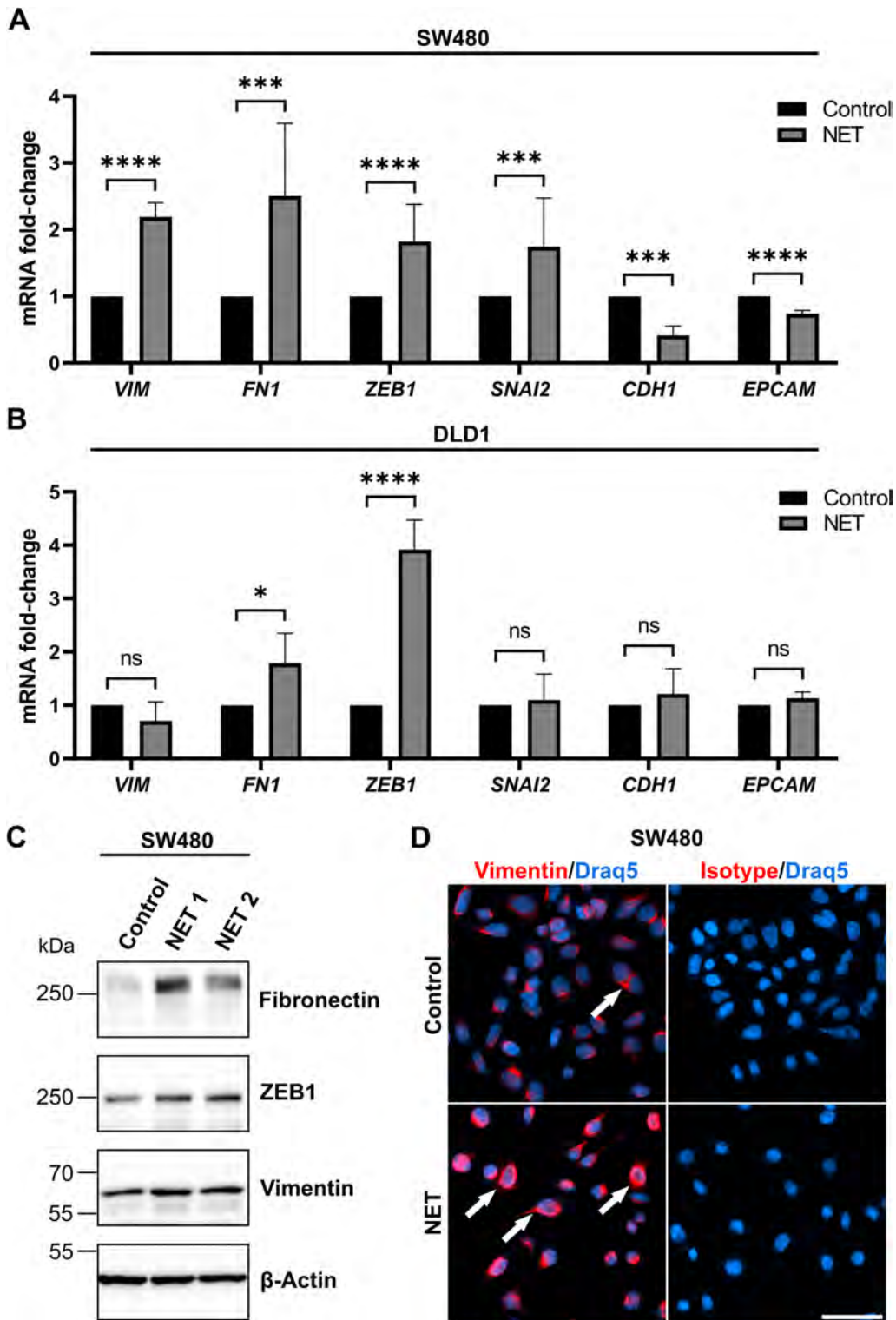
**Figure 5.** NETs induced EMT in CRC cell lines. (A, B) mRNA expression of *VIM*, *FN1*, *ZEB1*, *SNAI2*, *CDH1* and *EPCAM* in SW480 cells (A) and DLD1 cells (B) either unstimulated (Control) or after treatment with 500 ng/ml NETs for 12 h. Gene expression was normalised to *RPL37A* and is shown in fold-changes. Statistical significance was determined using two-sided, unpaired *t*-test. *$p < 0.05$; **$p < 0.01$; ***$p < 0.001$; ****$p < 0.0001$. (C) Detection of fibronectin, ZEB1 and vimentin by western blotting in SW480 cells cultivated in the absence (Control) or presence of NETs (500 ng/ml) for 12 h. NET 1 and NET 2 represent NETs generated from different donors and yielded comparable results. Levels of β-actin showed that equal amounts of protein were loaded. NETs increased the expression of fibronectin, ZEB1 and vimentin in SW480 cells. (D) Immunocytochemistry detected increased expression of vimentin in SW480 cells after stimulation with NETs (500 ng/ml) for 24 h as compared with unstimulated cells (Control). Nuclei were counterstained with Draq5. Staining with an isotype control antibody did not show any signal. Arrows indicate vimentin-expressing SW480 cells. Scale bar: 50 μm.

with the fact that DNA in NETs is less condensed and accordingly better accessible to the large IgM anti-DNA antibody as compared with highly condensed nuclear DNA. These results further supported the notion that H3cit staining is specifically associated with the citrullinated NETs in colon cancer tissues, whereas

Table 2. Differentiation of nuclear and extracellular NET-associated chromatin in colon cancer tissues.

| | H2B | Anti-DNA | DAPI | NE | H3cit |
|---|---|---|---|---|---|
| Nuclear, resting, condensed | + | − | ++ | − | − |
| Extracellular de-condensed | + | ++ | + | + | − |
| Extracellular citrullinated de-condensed (citrullinated NETs) | + | ++ | + | + | + |

overlapping signals for NE and H2B may also be derived from intact neutrophils. Profiling of the NE/H2B signal intensities confirmed this conclusion (Figure 1C). Optical sections of H3cit-positive tissues showed similar distribution of NE and H2B signals, indicating co-localisation of both molecules, a hallmark of NETs (Figure 1C, patient 1). In contrast, in specimens lacking H3cit the intensities of NE and H2B followed an opposite course, reaching maxima at different sites with an intersection at the nucleocytoplasmic transition zone (Figure 1C, patient 3). In total, we concluded that H3cit staining is sufficient to reliably detect citrullinated NETs in colon cancer tissues (Figure 1D).

## NETs are associated with high tumour grades and local metastasis in colon cancer

In order to translationally determine a potential association of NETs with specific clinical features in human colon cancer tissues, we analysed NE, H2B, H3cit and extranuclear DNA in a cohort of $n = 85$ patients (Table 1) using immunofluorescence microscopy. In agreement with the STED analysis, H3cit-positive sections exhibited high amounts of extranuclear DNA, as indicated by staining with an anti-DNA antibody (Figure 2A, left panels, arrows). In contrast, areas exhibiting merely NE/H2B staining in the absence of H3cit showed only low amounts of de-condensed DNA that can be detected by immunofluorescence microscopy (Figure 2A, right panels, asterisks).

Quantitative evaluation of the immunofluorescence analyses showed that NETs were more frequently present in colon tumours with higher grade (grade 3/4), locoregional metastasis (pN1/2) and consequently in UICC stage III (Figure 2B,C,E). In addition, NETs were more often observed in tumours with increased local invasion (Figure 2D). Finally, we evaluated whether NETs may appear at specific sites within the lesions. In most of the samples, NETs were detected either in the tumour centre and the invasive front (35.5%) or in the tumour centre only (32.3%) (Figure 3A, left panel, for tumour areas see Figure 3B). A minority of tumours showed NET formation in the tumour centre and the luminal side, in all three compartments or exclusively in the invasive front or the luminal site (Figure 3A, left panel). The localisation of NETs was comparable in high- and low-grade tumours (Figure 3A, right panel).

## NETs induce motility and epithelial–mesenchymal transition (EMT) in human CRC cell lines

Higher tumour grade has been shown to be associated with EMT, which describes the formation of a mesenchymal tumour cell phenotype with increased motility [32]. In order to investigate this in CRC cells, NETs were isolated from PMA-stimulated human neutrophils *in vitro*. CRC cell lines (DLD1, SW480) incubated with NETs changed their morphology, which was most clearly reflected by the formation of long pseudopodia (Figure 4A, arrows) and alterations of the actin cytoskeleton, detected by phalloidin staining (Figure 4A, right). Moreover, a wound healing assay showed that NETs significantly increased the migration of CRC cells (Figure 4B,C and supplementary material, Figure S2B). The increased migration of DLD1 and SW480 cells in the presence of NETs was also confirmed by time-lapse video microscopy (see supplementary material, Movie S1). Of note, NET formation was induced by the treatment of neutrophils with 0.5 μM PMA, which may activate cell migration *per se*. However, during NET isolation, until application onto tumour cells the PMA concentrations were highly diluted down to less than 7 pM. In control experiments, PMA even at 17-fold higher concentrations (100 pM) did not activate CRC cell migration (see Materials and methods and supplementary material, Figure S1). This finding excluded residual PMA in NET preparations being responsible for the activation of migration.

In order to investigate whether the DNA or protein content of NETs increased CRC cell motility, NETs were either digested with DNase I alone or in addition subjected to thermal treatment (95 °C, 20 min). Digestion with DNase I alone did not suffice to abrogate the effects of NETs on cancer cell motility. However, upon subsequent heat denaturation of NET proteins, migratory activity of DLD1 and SW480 cells was significantly lower as compared with stimulation with untreated NETs (Figure 4C and supplementary material, Figure S2B).

Increased motility of epithelial cells is often associated with EMT, characterised by a downregulation of epithelial markers and simultaneous upregulation of mesenchymal markers and EMT promoting transcription factors. Interestingly, in SW480 cells, incubation with NETs increased the expression of genes encoding the mesenchymal markers vimentin (*VIM*) and fibronectin (*FN1*) and of the transcription factors ZEB1 (*ZEB1*) and Slug (*SNAI2*) and decreased the expression of the epithelial markers E-cadherin (*CDH1*) and epithelial cell adhesion molecule (*EPCAM*) (Figure 5A). In DLD1 cells, a significant increase of *FN1* as well as *ZEB1* expression could be observed (Figure 5B). The three most highly expressed genes altered upon treatment with NETs (*FN1*, *ZEB1*, *VIM*) were validated at the protein level by western blotting (Figure 5C). Moreover, increased expression of vimentin in SW480 cells after stimulation with NETs was confirmed by immunofluorescence (Figure 5D).

## Discussion

We found that NETs are abundantly present in human colon cancer tissues and can specifically be detected by H3cit staining. The presence of NETs was associated with high histopathological tumour grades and lymph node metastases. Treatment of CRC cell lines with NETs induced a migratory phenotype with decreased expression of epithelial markers and increased expression of mesenchymal markers and EMT-promoting transcription factors. Thus, NETs induce an EMT-like phenotype and through this may actively contribute to tissue invasion and lymph node metastasis in colon cancer.

Recently published protocols suggested that NETs can be identified by co-localisation of NE and H2B, as in intact neutrophils both proteins reside in different cellular compartments; namely NE in the cytoplasmic granules and H2B in the nucleus [21]. Other studies used H3cit as a marker of NETs in tissues either solitary or in combination with other markers [18,19,25,33]. However, in solid tumours, arginine deimination (also referred to as citrullination) of histones has also been observed during epigenetic regulation of gene expression [34]. In agreement with this, PAD4 (the enzyme catalysing histone H3 citrullination) was reported to be frequently overexpressed in cancer cells [35]. Accordingly, a recent study used multiplex immunofluorescence combining the detection of H3cit with the granulocyte marker CD15 and the neutrophil marker MPO for the detection of NETs in various solid tumours [25]. However, multiplex analyses are difficult to integrate into routine diagnostic processes. In order to determine which marker may be the most appropriate to detect citrullinated NETs in colon cancer tissues, super resolution STED microscopy was applied here. We found that NE, H2B and H3cit co-localised in colon cancer tissues but NE/H2B co-localisation was clearly more common as compared with H3cit staining. The reason for this was that NE and H2B co-localisation was not specific for NETs and also appeared at the nucleocytoplasmic transition zone in intact neutrophils. This situation was demonstrated by signal intensity profiling. Interestingly, under the conditions used for immunofluorescence (FFPE tissues, target retrieval at pH 6.0, 20 min, 90 °C), DNA was strongly stained with an anti-DNA antibody in areas where H3cit was also detected. In these areas, DNA staining presented with a fibrous randomly scattered pattern indicating NETs. In contrast, strongly reduced or no signals were obtained with the anti-DNA antibody in cells with condensed nuclear DNA, as the high molecular weight IgM antibody (900 kDa) has limited penetration of condensed nuclear DNA. In contrast, the reactivity of the low molecular weight compound DAPI (0.28 kDa) preferred condensed nuclear DNA over extracellular, de-condensed DNA of NETs. In total, these observations suggested that the anti-DNA antibody reacts with extracellular de-condensed DNA of NETs, which reveals improved accessibility of respective epitopes as compared with highly condensed nuclear DNA. The coincidence of H3cit and extracellular DNA further confirmed that extracellular staining of H3cit is the most sensitive marker for citrullinated NETs in human colon cancer tissues (Table 2).

As yet, the relationship of NETs in primary tumour tissues with clinical parameters in colon cancer has not been investigated in larger patient cohorts. A putative role of NETs in cancer development has been suggested by murine models showing that surgical stress and increased LPS levels after postoperative infections lead to NET formation and increased occurrence of metastases [33,36]. In addition, high MPO DNA levels in the serum have been associated with increased risk of tumour relapse and shorter overall and disease-free survival [20,33,36]. In murine models of breast and colon cancer it has been shown that NETs in the liver and lungs actively attract cancer cells to form metastases by interaction of the transmembrane protein coiled-coil domain containing protein 25 (CCDC25) with NETs. CCDC25 on cancer cells hereby acted as a receptor for NET DNA [18]. The presence of NETs in the primary tumour tissue of patients with CRC was only shown in small cohorts of 10 and 20 patients [24,25]. To our knowledge, we are the first to systemically investigate the presence of NETs in primary colon cancer lesions on a large cohort of patients. Intra-tumoural citrullinated NETs were associated with high tumour grade, lymph node metastases and a trend towards local tumour progression. Our results support the clinical relevance and association with an unfavourable clinical course of citrullinated NETs in colon cancer, indicating that they contribute to disease progression.

In epithelial-derived solid tumours such as CRC, high tumour grade, lymph node metastasis and advanced clinical stage have been connected to EMT [37]. Studies on the relationship between NETs and EMT indicated that NETs promote a mesenchymal, pro-metastatic phenotype in breast [38], gastric [39] and pancreatic cancer [40] cell lines. In agreement with these previous studies on various tumours, our findings provided clear evidence that NETs exert a direct effect on CRC cells by increasing their migratory capabilities and inducing features of EMT, such as the increased expression of *VIM*, *FN1*, *ZEB1* and *SNAI2*, as well as the decreased expression of *CDH1* and *EPCAM*. Previous studies proposed the proteins of NETs as the main contributors to EMT induction [38,41,42]. In accordance with this, we noted that the EMT-associated migration cannot be abrogated by degradation of the NETs' DNA. Instead, the migration-inducing activity of NETs was found to be thermo-labile, supporting the hypothesis that it is triggered by proteins.

In conclusion, the detection of NETs by immunofluorescence using the combination of H3cit and anti-DNA antibodies provides a possibility to determine the prognosis of CRC patients. In addition, our results suggest that NETs are a putative therapeutic target, to decrease the risk of metastasis in patients with CRC.

## Acknowledgements

## Author contributions statement

AMS, MH and MS designed the experiments. AMS, RD, MPS, JS, PT and SV performed the experiments. AMS, GW, RD, MPS, PT, BS, SM, CB, EN, MH and MS analysed the data. PT, BS, CIG, AH, LEM, JS, CB, GS, RG and MH provided key reagents, materials, analysis tools and helpful ideas. AMS and MS wrote the manuscript. All authors approved the final version of the manuscript.

## References

1. Mattiuzzi C, Lippi G. Current cancer epidemiology. *J Epidemiol Glob Health* 2019; **9:** 217–222.

2. Galon J, Costes A, Sanchez-Cabo F, *et al*. Type, density, and location of immune cells within human colorectal tumors predict clinical outcome. *Science* 2006; **313:** 1960–1964.

3. Guinney J, Dienstmann R, Wang X, *et al*. The consensus molecular subtypes of colorectal cancer. *Nat Med* 2015; **21:** 1350–1356.

4. Jackstadt R, van Hooff SR, Leach JD, *et al*. Epithelial NOTCH signaling rewires the tumor microenvironment of colorectal cancer to drive poor-prognosis subtypes and metastasis. *Cancer Cell* 2019; **36:** 319–336 e7.

5. Nathan C. Neutrophils and immunity: challenges and opportunities. *Nat Rev Immunol* 2006; **6:** 173–182.

6. Brinkmann V, Reichard U, Goosmann C, *et al*. Neutrophil extracellular traps kill bacteria. *Science* 2004; **303:** 1532–1535.

7. Fuchs TA, Abed U, Goosmann C, *et al*. Novel cell death program leads to neutrophil extracellular traps. *J Cell Biol* 2007; **176:** 231–241.

8. Erpenbeck L, Schon MP. Neutrophil extracellular traps: protagonists of cancer progression? *Oncogene* 2017; **36:** 2483–2490.

9. Brill A, Fuchs TA, Savchenko AS, *et al*. Neutrophil extracellular traps promote deep vein thrombosis in mice. *J Thromb Haemost* 2012; **10:** 136–144.

10. Leppkes M, Knopf J, Naschberger E, *et al*. Vascular occlusion by neutrophil extracellular traps in COVID-19. *EBioMedicine* 2020; **58:** 102925.

11. Leffler J, Gullstrand B, Jonsen A, *et al*. Degradation of neutrophil extracellular traps co-varies with disease activity in patients with systemic lupus erythematosus. *Arthritis Res Ther* 2013; **15:** R84.

12. Khandpur R, Carmona-Rivera C, Vivekanandan-Giri A, *et al*. NETs are a source of citrullinated autoantigens and stimulate inflammatory responses in rheumatoid arthritis. *Sci Transl Med* 2013; **5:** 178ra140.

13. Gupta AK, Hasler P, Holzgreve W, *et al*. Induction of neutrophil extracellular DNA lattices by placental microparticles and IL-8 and their presence in preeclampsia. *Hum Immunol* 2005; **66:** 1146–1154.

14. Yipp BG, Petri B, Salina D, *et al*. Infection-induced NETosis is a dynamic process involving neutrophil multitasking in vivo. *Nat Med* 2012; **18:** 1386–1393.

15. Ackermann M, Anders HJ, Bilyy R, *et al*. Patients with COVID-19: in the dark-NETs of neutrophils. *Cell Death Differ* 2021; **28:** 3125–3139.

16. Berger-Achituv S, Brinkmann V, Abed UA, *et al*. A proposed role for neutrophil extracellular traps in cancer immunoediting. *Front Immunol* 2013; **4:** 48.

17. Park J, Wysocki RW, Amoozgar Z, *et al*. Cancer cells induce metastasis-supporting neutrophil extracellular DNA traps. *Sci Transl Med* 2016; **8:** 361ra138.

18. Yang L, Liu Q, Zhang X, *et al*. DNA of neutrophil extracellular traps promotes cancer metastasis via CCDC25. *Nature* 2020; **583:** 133–138.

19. Albrengues J, Shields MA, Ng D, *et al*. Neutrophil extracellular traps produced during inflammation awaken dormant cancer cells in mice. *Science* 2018; **361:** eaao4227.

20. Yazdani HO, Roy E, Comerci AJ, *et al*. Neutrophil extracellular traps drive mitochondrial homeostasis in tumors to augment growth. *Cancer Res* 2019; **79:** 5626–5639.

21. Abu Abed U, Brinkmann V. Immunofluorescence labelling of human and murine neutrophil extracellular traps in paraffin-embedded tissue. *J Vis Exp* 2019; **151:** e60115.

22. Lewis HD, Liddle J, Coote JE, *et al*. Inhibition of PAD4 activity is sufficient to disrupt mouse and human NET formation. *Nat Chem Biol* 2015; **11:** 189–191.

23. Biron BM, Chung CS, O'Brien XM, *et al*. Cl-amidine prevents histone 3 citrullination and neutrophil extracellular trap formation, and improves survival in a murine sepsis model. *J Innate Immun* 2017; **9:** 22–32.

24. Arelaki S, Arampatzioglou A, Kambas K, *et al*. Gradient infiltration of neutrophil extracellular traps in colon cancer and evidence for their involvement in tumour growth. *PLoS One* 2016; **11:** e0154484.

25. de Andrea CE, Ochoa MC, Villalba-Esparza M, *et al*. Heterogenous presence of neutrophil extracellular traps in human solid tumours is partially dependent on interleukin-8. *J Pathol* 2021; **255:** 190–201.

26. Brierley JD, Gospodarowicz MK, Wittekind C. *The TNM Classification of Malignant Tumours* (8th edn). Wiley Blackwell: Oxford, 2017.

27. Langer V, Vivi E, Regensburger D, *et al*. IFN-gamma drives inflammatory bowel disease pathogenesis through VE-cadherin-directed vascular barrier disruption. *J Clin Invest* 2019; **129:** 4691–4707.

28. Naschberger E, Liebl A, Schellerer VS, *et al*. Matricellular protein SPARCL1 regulates tumor microenvironment-dependent endothelial cell heterogeneity in colorectal carcinoma. *J Clin Invest* 2016; **126:** 4187–4204.

29. Najmeh S, Cools-Lartigue J, Giannias B, *et al*. Simplified human neutrophil extracellular traps (NETs) isolation and handling. *J Vis Exp* 2015; **98:** 52687.

30. Stürzl M, Gaus D, Dirks WG, *et al*. Kaposi's sarcoma-derived cell line SLK is not of endothelial origin, but is a contaminant from a known renal carcinoma cell line. *Int J Cancer* 2013; **132:** 1954–1958.

31. Weinländer K, Naschberger E, Lehmann MH, *et al*. Guanylate binding protein-1 inhibits spreading and migration of endothelial cells through induction of integrin alpha4 expression. *FASEB J* 2008; **22:** 4168–4178.

32. Lahat G, Lubezky N, Loewenstein S, *et al*. Epithelial-to-mesenchymal transition (EMT) in intraductal papillary mucinous

neoplasm (IPMN) is associated with high tumor grade and adverse outcomes. *Ann Surg Oncol* 2014; **21**(Suppl 4): S750–S757.

33. Tohme S, Yazdani HO, Al-Khafaji AB, *et al*. Neutrophil extracellular traps promote the development and progression of liver metastases after surgical stress. *Cancer Res* 2016; **76**: 1367–1380.

34. Wang Y, Chen R, Gan Y, *et al*. The roles of PAD2- and PAD4-mediated protein citrullination catalysis in cancers. *Int J Cancer* 2021; **148**: 267–276.

35. Yuzhalin AE. Citrullination in cancer. *Cancer Res* 2019; **79**: 1274–1284.

36. Wang WW, Wu L, Lu W, *et al*. Lipopolysaccharides increase the risk of colorectal cancer recurrence and metastasis due to the induction of neutrophil extracellular traps after curative resection. *J Cancer Res Clin Oncol* 2021; **147**: 2609–2619.

37. Luo Y, Yu T, Zhang Q, *et al*. Upregulated N-cadherin expression is associated with poor prognosis in epithelial-derived solid tumours: a meta-analysis. *Eur J Clin Invest* 2018; **48**: e12903.

38. Martins-Cardoso K, Almeida VH, Bagri KM, *et al*. Neutrophil extracellular traps (NETs) promote pro-metastatic phenotype in human breast cancer cells through epithelial-mesenchymal transition. *Cancers (Basel)* 2020; **12**: 1542.

39. Zhu T, Zou X, Yang C, *et al*. Neutrophil extracellular traps promote gastric cancer metastasis by inducing epithelialmesenchymal transition. *Int J Mol Med* 2021; **48**: 127.

40. Jin W, Yin H, Li H, *et al*. Neutrophil extracellular DNA traps promote pancreatic cancer cells migration and invasion by activating EGFR/ERK pathway. *J Cell Mol Med* 2021; **25**: 5443–5456.

41. Yang D, Liu J. Neutrophil extracellular traps: a new player in cancer metastasis and therapeutic target. *J Exp Clin Cancer Res* 2021; **40**: 233.

42. Kajioka H, Kagawa S, Ito A, *et al*. Targeting neutrophil extracellular traps with thrombomodulin prevents pancreatic cancer metastasis. *Cancer Lett* 2021; **497**: 1–13.

---

## SUPPLEMENTARY MATERIAL ONLINE

**Supplementary materials and methods**

**Supplementary figure legends**

**Figure S1.** Increased migration of DLD1 cells upon stimulation with NETs is not due to residual PMA

**Figure S2.** Increased migration of SW480 cells upon simulation with NETs can be abrogated by digestion of NETs with DNase and subsequent heat inactivation, but not by digestion with DNase alone

**Movie S1.** Time-lapse video microscopy of DLD1 and SW480 tumour cells untreated (Control) and in the presence of NETs